2015

Investigating the Role of Bptf in Immunoediting in Breast Cancer and Melanoma

Kristen N. Peterson
Virginia Commonwealth University, petersonkn@vcu.edu

INVESTIGATING THE ROLE OF BPTF IN IMMUNOEDITING IN BREAST CANCER AND MELANOMA

A thesis submitted in partial fulfillment of the requirements for the degree of Master of Science at Virginia Commonwealth University

by

Kristen Nichole Peterson
Bachelor of Science, University of Kentucky, 2011

Director: Joseph W. Landry, Ph.D.
Assistant Professor
Department of Human and Molecular Genetics

Virginia Commonwealth University
Richmond, Virginia
April 2015

ACKNOWLEDGEMENT

First and foremost, I would like to thank my parents, Richard and Kathleen Snyder, for not only entertaining, but encouraging my natural curiosity, and for providing unwavering support, strength, and love throughout my life. I would also like to thank my husband, Michael, for being someone to listen and bounce ideas off of, for being honest with me (when those ideas weren't best), for providing a shoulder to cry on when I felt I wasn't strong enough to take on any challenge, and for being a constant source of love and laughter.

A huge thanks is also owed to Kimberly Mayes, my lab mate and unofficial mentor. You taught me countless techniques, guided my studies so I would get the most out of my time as a Master's student, ensured I understood the decision process behind experiments, and never failed to answer my countless questions and correct my thought process when I got carried away. I will always be grateful for the compassion and patience you showed.

I would also like to thank my advisor, Dr. Joseph Landry, for the opportunity to complete my thesis work in his lab, as well as my fellow lab members Marissa and Aiman, who provided assistance and laughter throughout the past two years, making lab each day that much more enjoyable.

Finally, I would like to thank my committee members, Drs. Xiang-Yang (Shawn) Wang and Tomasz Kordula, for providing feedback on my research and suggesting ways to improve my work.

TABLE OF CONTENTS

LIST OF TABLES AND FIGURES

LIST OF ABBREVIATIONS

7AAD – 7-amino-actiomycin D

aa – Amino acid

APC – Antigen presenting cell

ATP – Adenosine-tri-phosphate

B2M – Beta-2 microglobulin

BALB/c – Bagg albino (inbred mouse strain)

bp – Base pair

BPTF – Bromodomain PHD-finger containing transcription factor

CD – Cluster of differentiation marker

cm – Centimeter

CO2 – Carbon dioxide

diH2O – Deionized water

DMEM – Dulbecco's modified eagle medium

DNA – Deoxyribonucleic acid

DP – Double positive

ECL – Enhanced chemiluminescence

EDTA – Ethylenediaminetetraacetic acid

ELISA – Enzyme-linked immune assay

ER – Endoplasmic reticulum

ESC – Embryonic stem cell

FBS – Fetal bovine serum

FITC – Fluorescein isothiocyanate

HBSS – Hank's balanced salt solution

IFN – Interferon

KD – Knock-down

KO – Knock-out

LDH – Lactase dehydroenase

LMP – Low-molecular mass polypeptide

mA – Milliamp

mAb – Monoclonal antibody

MEF – Mouse embryonic fibroblast

MFI – Mean fluorescence intensity

MHC – Major histocompatibility complex

NEAA – Non-essential amino acids

NFDM – Non-fat dry milk

NK – Natural killer

NSG – NOD/SCID, IFNg2r -/- (mouse strain)

NURF – Nucleosome remodeling factor

ova – Ovalbumin

PE – R-Phycoerythrin

Pmel – Premelanosome protein

PVDF – Polyvinylidene fluoride

qPCR – Quantitative polymerase chain reaction

RBC – Red blood cell

rpm – Revolutions per minute

SWI/SNF – Switch/sucrose non-fermentable

TAP – Transporter associated with antigen processing

TCR – T cell receptor

TCRβ – T cell beta chain

V – Volt

ABSTRACT

INVESTIGATING THE ROLE OF BPTF IN IMMUNOEDITING IN BREAST CANCER AND MELANOMA

by Kristen Nichole Peterson, B.S

A thesis submitted in partial fulfillment of the requirements for the degree of Master of Science at Virginia Commonwealth University

Virginia Commonwealth University, 2015

Major Director: Joseph W. Landry
Assistant Professor, Department of Human and Molecular Genetics

In this study, we explore the effects of NURF depletion on the growth of tumors in immune-competent mice. NURF depletion in tumors results in reduced tumor growth in immune-competent mice, suggesting enhanced anti-tumor immunity. Analysis of the tumor microenvironment by flow cytometry revealed a significantly elevated CD8 and progressively elevated activated CD8 phenotype in Bptf KD tumors, possibly contributing to the increase in cell death and decrease in tumor weight observed. Examination of antigen presentation was evaluated using the OT-1 and Pmel-17 models, though no significant difference in cytotoxicity was observed as measured by LDH and/or IFNγ assays. This indicates possible novel antigen presentation mechanisms in tumor cells, and not increased presentation of existing antigens, contributes to the decreased tumor weight observed in Bptf KD tumors.

INTRODUCTION

Cancer affects millions of people worldwide each year. Even considering the great advances made in the past 25 years, resulting in a 10-18% decrease in death rate, 1 in 4 deaths in the United States continues to be attributed to cancer [1]. With these statistics looming over us, it's no surprise that the research community has been focused on not only what causes cancer, but how to overcome or even cure cancer for future generations. Immunotherapies, a relatively new concept focusing on the ability to manipulate and take advantage of our body's existing defense mechanisms, have gained notoriety with their ability to mitigate diseases that previously had a grim outlook and little to no available therapy. Today's immunotherapies include both passive and active immunotherapies, with passive therapies encompassing tumor-targeting monoclonal antibodies (mAbs), adoptive cell transfer (ACT), and oncolytic viruses, and active immunotherapies including many anticancer vaccines, dendritic cell based therapies, immunomodulatory mAbs, and introduction of immune-stimulating cytokines [2,3,4,5,6]. Although current immunotherapies have made great strides in modern medicine and research, there are still many avenues yet to be exploited. One area of research harboring potential therapeutics is epigenetics and its included chromatin remodelers.

Epigenetics

Deoxyribonucleic acid (DNA), the hereditary material of life, is present in the nucleus of every cell; with a single cell being only 5-6μm in diameter on average, a significant amount of compaction must occur to fit approximately 6 feet of DNA into the nucleus [7]. In order to

complete this compaction, DNA goes through a series of folding to create a complex structure called chromatin (Figure 1). At its fundamental level, approximately 150 base pairs (bp) of DNA then wrap around a histone octamer core 1.7 times, forming a nucleosome [7,8]. Nucleosomes continue to fold tightly on themselves, creating a chromatin fiber, which can further fold into a chromosome that is visible during metaphase.

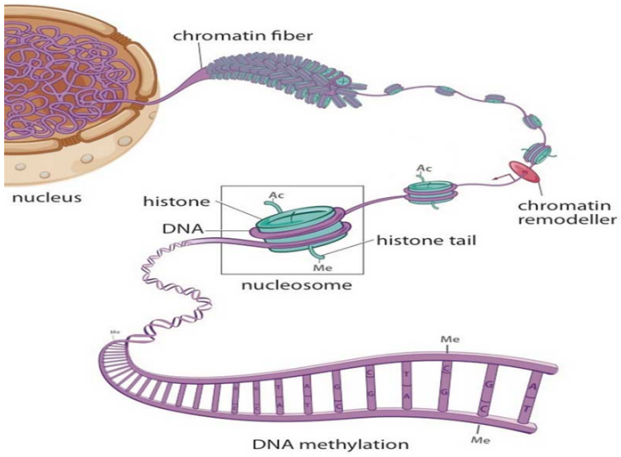

Figure 1: Compaction of DNA Inside the Nucleus. DNA is compacted into chromatin, the basic unit of which is the nucleosome. [9]

While chromatin provides a means for DNA to fit inside the nucleus, it also presents a problem; approximately 80 percent of DNA is wrapped around nucleosomes, and the segments of DNA wrapped around these histone octamers are generally inaccessible to transcription factors which are required for gene expression [10]. Epigenetics solves this problem with the introduction of histone variants and reversible modifications on histones including methylation, acetylation, and phosphorylation. These histone modifications are then recognized in part by chromatin remodeling complexes. In one example, the SWI/SNF family of chromatin remodeling complexes slides the nucleosome 10 bp in either direction in an adenosine triphosphate (ATP)-dependent manner, thereby exposing previously inaccessible sites [11,12].

Exposure of inaccessible sites allows transcription factor binding which can in turn regulate transcription.

NURF

Nucleosome Remodeling Factor (NURF), a member of the ISWI family of chromatin remodeling complexes, slides the nucleosome in 10 bp increments onto a thermodynamically stable position of DNA sequence [11,12,13]. For nucleosome remodeling by NURF to occur, the tail of histone H4 must be present, as well as its N-terminal residues [14]. NURF consists of three distinct subunits; the Bromodomain PHD-finger containing transcription factor (Bptf), the largest subunit, the ATPase SNF2L, and the pRBAP46/48 subunit containing a tryptophan-aspartic acid (WD) repeat combine to create the human form of NURF (Figure 2) [8].

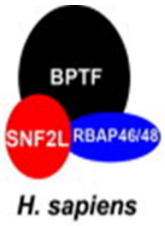

Figure 2: The NURF Complex in Humans. The NURF complex in humans consists of the Bptf, SNF2L, and pRABP46/48 subunits. [8]

Previous work has shown the subunit Bptf to be unique to NURF, making it the preferred candidate to manipulate for studies of this chromatin remodeler [8]. Bptf plays a role in mouse embryogenesis as well as thymocyte maturation, and has been shown to be embryonic lethal, but is not cell essential [15,16]. These characteristics highlight the importance of Bptf while illustrating its potential as a therapeutic agent against cancer.

NURF in Cancer

The gene encoding the Bptf subunit of NURF is located on the long arm of chromosome 17 [2]. Previous studies have demonstrated this arm of chromosome 17 is duplicated frequently in primary human cancers including breast, brain, liver, and lung cancers, implicating Bptf may play a role in tumorigenesis [17,18,19,20]. One study has identified a non-reciprocal translocation (der(X)t(X;17)) in lung cells maintained in continuous culture that occurs within the Bptf gene, and further showed elevated Bptf messenger ribonucleic acid (mRNA) levels and increased cell proliferation in cells containing this translocation [21].

Tumorigenesis

Tumorigenesis occurs when cells that functioned normally no longer respond to growth and differentiation control mechanisms. Tumors begin when a single cell obtains a sustainable genetic mutation that increases its ability proliferate when it would typically be eliminated [22]. This hyperplastic cell continues to proliferate, creating a population of cells with similar genetic makeup. At some point, possibly years later, one of these hyperplastic cells can acquire an additional genetic mutation, resulting in further abnormal growth and appearance, and the establishment of cancerous cells [22,23]. These cancerous cells may continue to acquire mutations that will allow them to become invasive and likely metastatic.

Accumulation of mutations in cancer cells provides them with the characteristics required to evade established proliferation control mechanisms. These characteristics include self-sufficiency for growth signals, insensitivity to anti-proliferative signals, and evasion of

apoptosis, among others [24]. One mechanism for the continued growth of cancer cells is avoidance of detection and destruction by the immune system [25, 26, 27].

Role of the Immune System

A major player in the recognition of harmful cells within an organism is the body's immune system. The adaptive immune system comes into play when the body's innate, or immediate, immune system is overwhelmed and cannot fully eliminate its intended target [28]. The adaptive immune system consists of a variety of specialized cells that sample the surrounding environment and present the information to effector cells capable of responding appropriately [29].

Antigen presenting cells (APCs) such as macrophages and dendritic cells, members of the innate immune system, sample the environment by endocytosis [30]. Information taken in is then processed and presented on the surface of the cell as a peptide in complex with a Major Histocompatibility Complex (MHC) molecule. APCs then travel to a peripheral lymphoid organ, such as a lymph node, where they interact with and activate effector T cells recognizing the specific antigen presented [31].

The effector cells of the adaptive immune system include cluster of differentiation marker (CD) 4 and CD8 T cells. CD4 and CD8 T cells become activated when their surface T-cell receptor (TCR) interacts with the peptide:MHC complex on the APC [32]. While CD4 cells, also known as helper T cells, assist in the activation or production of other immune cells to eliminate pathogens, CD8 cells or cytotoxic T lymphocytes have both direct and indirect cytotoxicity mechanisms.

CD8 cells eliminate pathogens and infected cells by inducing apoptosis. Induction of apoptosis is achieved through a variety of mechanisms including induction of the Fas/TRAIL pathway [32], release of cytotoxic granules including perforin and granzyme [32], or cytokines such as interferon (IFN)-γ [33]. While cytotoxic granule release induces apoptosis by forming holes in target cell membranes and activating caspases in the target cell that eventually act to degrade target cell DNA [28,33], IFN-γ acts by increasing MHC Class I molecule levels on the target cell surface [34]. Increase of MHC Class I levels increases the likelihood a target cell will be recognized and apoptosis induced. IFN-γ also activates APCs and recruits them to the site of interest [28].

The activation of effector T cells depends on the recognition of a specific antigen by the TCR, as previously mentioned. This antigen is presented to the TCR by the peptide:MHC complex on the APC's cell surface [31]. In addition to their effector functions, CD4 and CD8 cells differ in the class of MHC molecule they recognize, with CD4 cells recognizing antigen presented by MHC Class II molecules and CD8 cells recognizing antigen presented by MHC Class I molecules [28]. NURF has been shown to preferentially regulate nucleosome occupancy across the MHC locus over other sites in the genome, implying it may have a role in regulating gene expression at the MHC, thereby regulating its activity (Figure 3A) [35]. Consistent with this model were observed significant changes in genes around MHC in multiple cells including embryonic stem cells (ESCs), mouse embryonic fibroblasts (MEFs), and double positive (DP) thymocytes with knock-out (KO) of Bptf (Figure 3B).

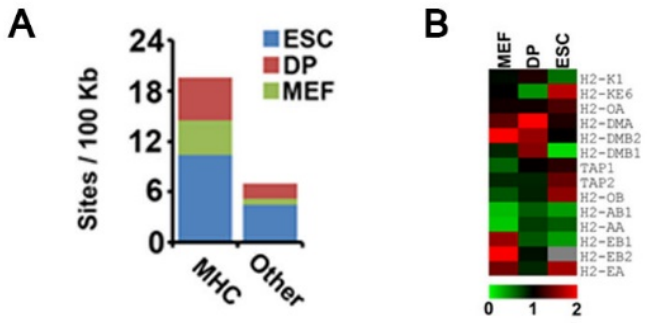

Figure 3: NURF Regulation of the MHC Locus and Associated Genes. (A) NURF preferentially regulates nucleosome occupancy across the MHC as compared to other loci in multiple cell types including embryonic stem cells (ESC), double positive thymocytes (DP), and mouse embryonic fibroblasts (MEF). (B) Microarray data from MEF, DP thymocyte, and ESC Bptf KDs show dysregulation of genes involved in tumorigenesis and antigen processing. Antigen processing genes shown include the TAP genes located within MHC genes at the MHC locus.

MHC Class I Peptide Presentation

Presentation of peptides on the cell surface of APCs via MHC molecules is regulated by a complex known as the proteasome in conjunction with the transporter associated with antigen process (TAP) complex [36]. The proteasome is responsible for degrading proteins into peptide fragments that are then transported from the cytosol into the endoplasmic reticulum (ER) via the TAP complex [37,38]. MHC Class I molecules preferentially present peptides of 8 to 11 amino acids in length [39]. When the proteolytic subunits of the proteasome core are replaced by the LMP2 and LMP7 catalytic subunits, the immunoproteasome is formed [40,41]. Immunoproteasome formation is induced by interferons and leads to a different cleavage pattern preference [40,41,42]. This differential cleavage pattern results in increased generation of peptides with a hydrophobic base and basic COOH termini – peptide fragments that are favored

by the TAP complex for uptake into the ER and have optimal binding to MHC Class I molecules (Figure 4) [40,41,43].

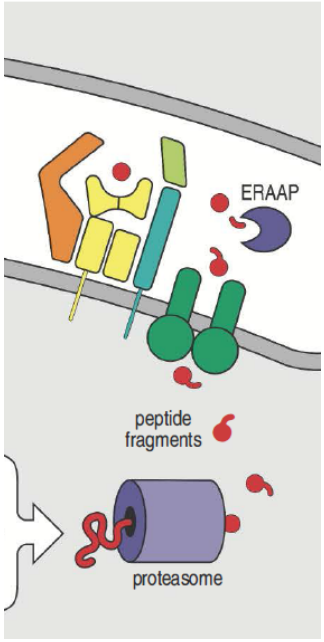

Figure 4: MHC Class I Antigen Processing. Proteins are broken down into peptide fragments in the cytosol (gray) by the proteasome. Peptide fragments are transported into the endoplasmic reticulum (white) by the TAP complex (green) for presentation on MHC Class I molecules (yellow) [28].

Previous Work in the Landry Lab

To begin investigating the role of Bptf in cancer, the Landry Lab injected cancer cell lines with control or Bptf shRNA retrovirus introduced knock down (KD) into the fourth mammary fat pad or flank of the respective syngeneic mouse strain. The two separate cancer cell lines and their derived tumors used were 4T1 and B16F10. The first cell line, 4T1, is an animal model for stage IV human breast cancer [44]. 4T1 cells grow in BALB/c mice and generate extremely tumorigenic and invasive tumors that can spontaneously metastasize from the site of the primary tumor to a variety of distant sites including lymph nodes, liver, lung, and brain [45].

Because of its metastatic characteristics, as well as the ability to remove the primary tumor surgically [46], 4T1 cells provide a reasonable mouse model for studying human breast cancer and has such become well characterized and frequently used in cancer research [47, 48, 49]. Another cancer cell line used was B16F10. B16F10 cells grow in C57BL/6 mice and are a well-established and frequently used mouse model for melanoma [50] and, similar to 4T1, are capable of spontaneously metastasizing to sites such as lymph nodes, lung, and brain [51, 52].

Previous work in the lab involving the injection of 4T1 Bptf KD and control cell lines into the fourth mammary fat pad of BALB/c mice which resulted in a significant decrease in the weight of Bptf KD tumors compared to tumors derived from control cell lines (Figure 5A). However, when injected into immune compromised NSG mice, a return to control phenotype of the tumors was observed, implicating the immune system as a major contributor to the decreased weight of Bptf KD tumors (Figure 5B). Similar studies using the B16F10 tumor model show reduced tumor sizes when Bptf KD cells are introduced into the flank of immune competent C57BL/6 mice (Figure 5C).

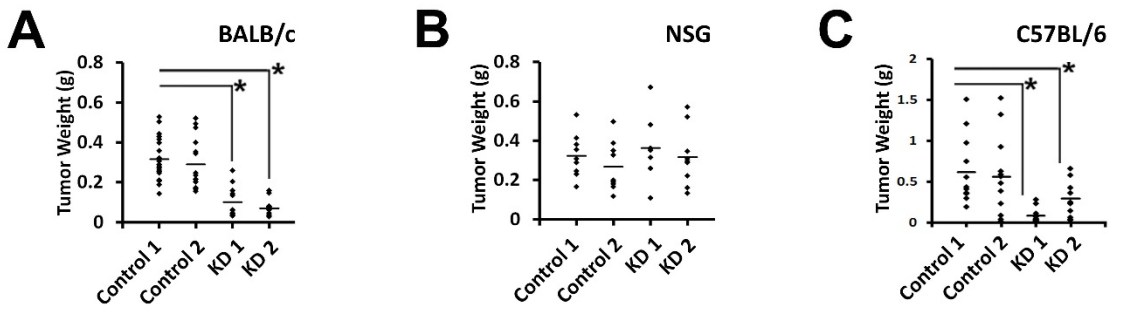

Figure 5: Weights of Bptf KD Tumors Decreased in BALB/c and C57BL/6 but not NSG Mice. (A) 4T1 Bptf KD cell lines injected into the fourth mammary fat pad of immune competent BALB/c mice created tumors of significantly decreased weight as compared to controls. (B) Reappearance of control phenotype in Bptf KD tumors when 4T1 cell lines were injected into immune deficient NSG mice. (C) B16F10 Bptf KD cell lines injected into the flank of immune competent C57BL/6 mice were significantly decreased in weight as compared to controls.

In addition to the return to control phenotype observed in immune compromised mice, previous data demonstrating that NURF preferentially occupies the MHC locus strongly implicated the immune system playing a critical role in the molecular mechanism behind the observed decreased weight of Bptf KD tumors [35]. The MHC locus is also known to include TAP and LMP genes [43]. Armed with all of this information, microarray data was collected to determine what genes may be dysregulated in Bptf KD cells. Results from these experiments illustrated dysregulation of a variety of genes, most interesting of which were upregulation of the TAP and LMP genes.

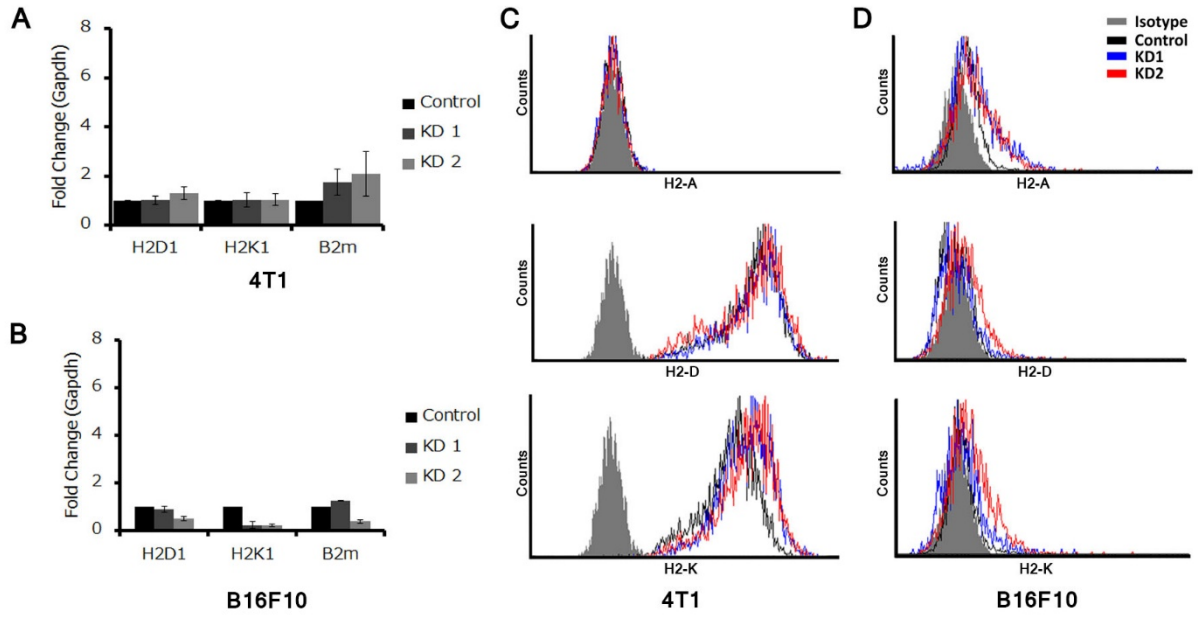

Figure 6: Similar MHC Class I Expression in Bptf Control and KD Cells. (A) qPCR analysis of the MHC Class I genes H2D1, H2K1, and B2m in 4T1 showing no significant difference between control and Bptf KD lines. (B) qPCR analysis in B16F10 showing no significant difference between control and Bptf KD lines. (C,D) Flow cytometry analysis of MHC Class I expression molecules including H2-A, H2-D, and H2-K in both 4T1 and B16F10 lines. Upregulation of H2-K is seen in 4T1, and upregulation of both H2-K and H2-D are seen in B16F10. Isotype is shown in gray, control in black, and two separate Bptf KD lines shown in blue and red.

With TAPs and LMPs play a role in MHC Class I antigen processing, studies were conducted to determine if these upregulated genes correlated with an increase in MHC Class I expression on the cell surface. Flow cytometry analysis of protein levels showed an increase H2-K in 4T1, and an increase in both H2-K and H2-D in B16F10 (Figure 6). These results were inconsistent with mRNA levels measured using qPCR. Data obtained through qPCR revealed that none of the MHC Class I genes in mice, including H2-K, H2-D, and β2-microglobulin (B2M), had significantly different expression levels in Bptf KD cell lines when compared to controls (Figure 6).

Microarray data was also confirmed by quantitative polymerase chain reaction (qPCR), showing an upregulation of *TAP1, TAP2, LMP2,* and *LMP7* in 4T1 and B16F10 cell lines with Bptf KD as compared to controls (Figure 7).

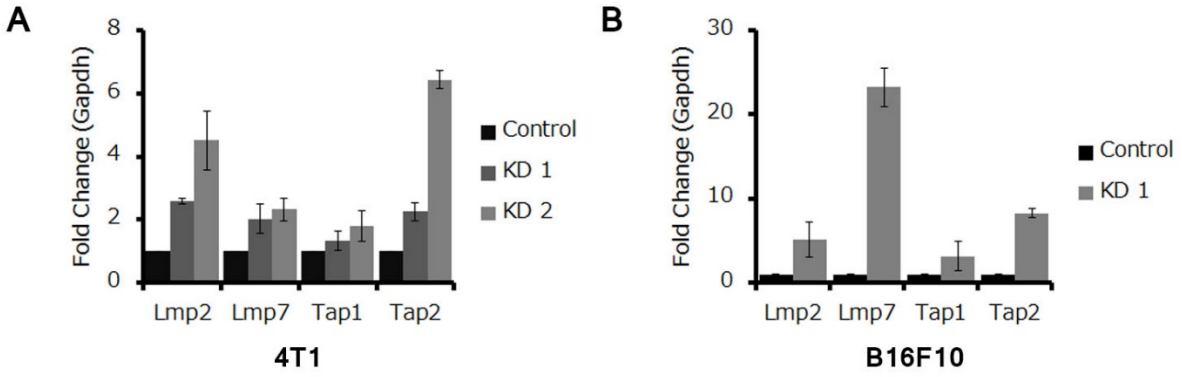

Figure 7: Upregulation of MHC Class I Antigen Processing Associated Genes. (A) qPCR analysis of antigen processing genes associated with MHC Class I antigen presentation showing a significant increase in expression of the Lmp2, Lmp7, Tap2, and Tap2 genes in 4T1 Bptf KD cells as compared to control. (B) Similar qPCR performed on B16F10 cells showing a significant increase in expression of Lmp2, Lmp7, Tap1, and Tap2 in Bptf KD as compared to control.

Data was collected showing the importance of CD8 T cells in obtaining the phenotypic difference between Bptf KD and control tumors. Through systematic depletion of CD4, CD8, and natural killer (NK) cells using antibodies against each of the cell types, it was revealed that CD4 and CD8 cells are required in the mechanisms at play in Bptf KD cells. This is illustrated in Figure 8, which shows a reappearance of control phenotype in Bptf KD tumors when mice were depleted of either CD4 or CD8 T cells.

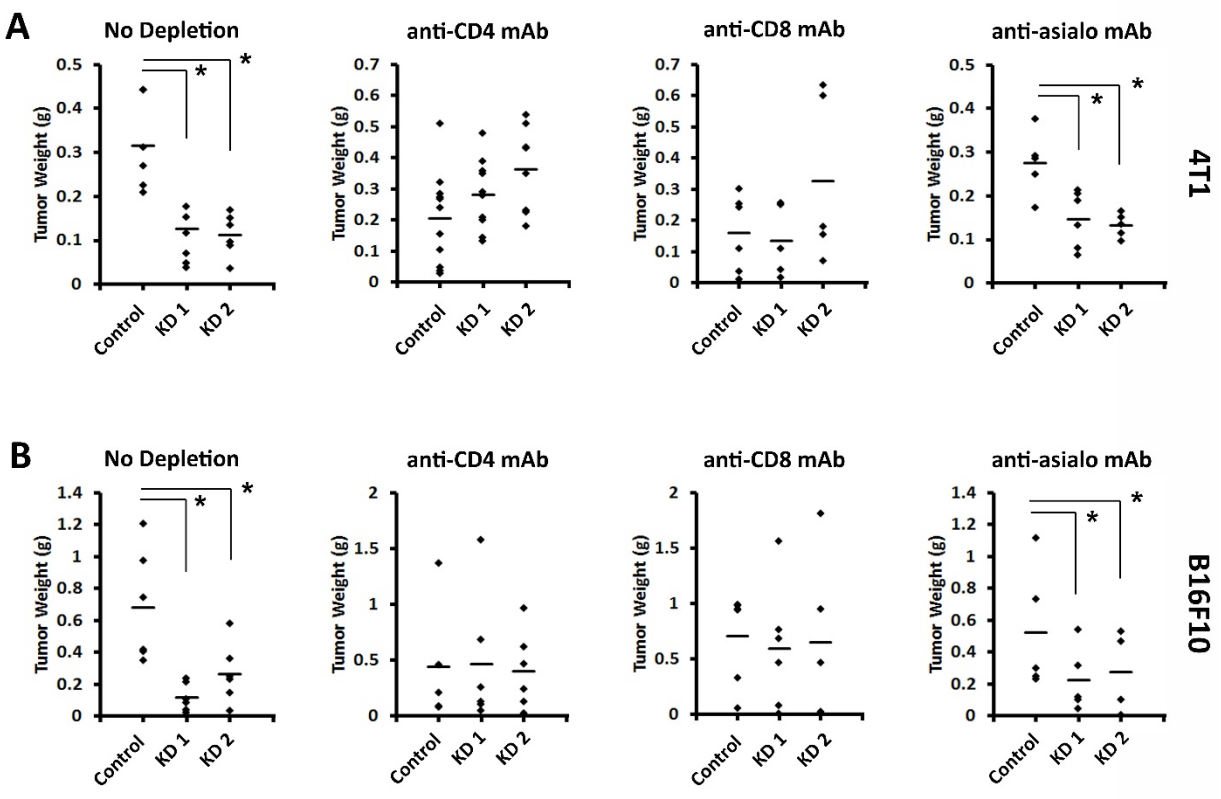

Figure 8: Systematic Depletion of CD4 and CD8 Cells Diminishes Reduced Growth of Bptf KD Tumors. (A,B) Systematic depletion of CD4, CD8, and NK cells using monoclonal antibodies against each, showing reappearance of control phenotype in Bptf KD lines when CD4 or CD8 T cells are depleted in both 4T1 and B16F10.

Lactate dehydrogenase (LDH) and IFN-γ cytotoxicity assays also provided evidence suggesting that CD8 T cells are important in Bptf KD tumor regression. To measure cell death by LDH cytotoxicity assay, supernatants from cultures containing target (tumor) cells in the presence of effector (CD8+ T cells) are obtained. LDH is a stable cytosolic enzyme that is released from cells upon cell lysis [61] into the culture supernatant. When placed in the presence of tetrazolium salt, the NADH released via LDH is oxidized, and a red formazan product is formed. Presence of red formazan product as detected by absorbance at 490nm is proportional to the number of cells lysed.

When released by activated CD8 T cells, IFN-γ is able to bind to its receptor and activate downstream pathways such as the JAK-STAT pathway and further induce apoptosis [62]. An ELISA assay specific for mouse IFN-γ was performed using culture supernatants from control and Bptf KD cells in the presence of CD8 T cells. To detect IFN-γ presence, cells are placed in primary capture antibody, a following secondary detection antibody, placed in the presence of Avidin-horseradish peroxidase (HRP), and finally combined with tetramethylbenzidine (TMB) substrate solution. The addition of Avidin-HRP produces hydrogen peroxide which, in the presence of TMB, oxidizes TMB and creates a soluble blue reaction product, turning the reaction solution from red to blue [63]. Analysis of the presence of blue reaction product is detected by absorbance at 450 nm and is proportional to the presence of IFN-γ released by CD8 T cells.

Results from these assays demonstrated that CD8 T cells obtained from the spleen of a BALB/c (for 4T1) mouse and primed on Bptf KD targets are able to kill Bptf KD tumor cells more effectively than CD8 cells primed on control targets are able to kill control tumor cells (Figure 9).

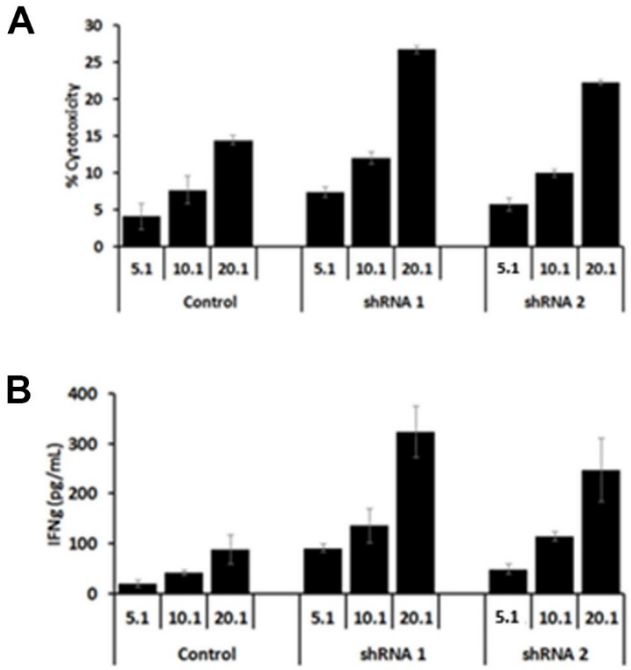

Figure 9: CD8+ T Cells Show Enhanced Killing of Bptf KD Tumor Cells. (A) LDH and (B) IFN-γ cytotoxicity assays reveal CD8+ T cells kill Bptf KD cells (shRNA 1 and 2) more efficiently than control cells. Ratios shown (5.1, 10.1, 20.1) represent the effector to target ratios utilized.

This data illustrates the likelihood of antigen presentation as well as CD8 cells playing critical roles in the difference in tumor regression between Bptf KD and control tumors.

Hypothesis/Aims of the Study

We have shown through antibody depletion and cytotoxicity assays, that CD8 T cells are crucial for Bptf KD tumor regression, however little is known about the CD8 T cell population phenotype *in vivo*. **Our first aim is to determine if Bptf KD tumors showed differential recruitment or activation of CD8 T cells in comparison to control tumor cells. We hypothesize that Bptf KD tumors will show a more activated CD8 T cell population when compared to control tumor cells.**

It has previously been shown that Bptf preferentially occupies the MHC locus. Microarray and qPCR data have also revealed that Bptf upregulates genes involved in antigen processing and presentation for MHC Class I molecules (i.e. TAPs and LMPs). It is, however, unknown whether Bptf KD tumor cells present antigen on their cell surface with greater efficiency or if they instead present novel antigens to CD8 T cells. **In our second aim, we hypothesize that Bptf KD tumor cells will show similar antigen presentation as controls, indicating novel antigen presentation is the likely mechanism for the observed Bptf KD tumor phenotype**.

MATERIALS AND METHODS

Cell Culture and Maintenance

Mouse breast cancer (4T1 from Fred Miller, Wayne State University) and melanoma (B16F10 from ATCC) cell lines were maintained in Dulbecco's Modified Eagle's Medium (DMEM) (Gibco) supplemented with 10% fetal bovine serum (FBS), 1X non-essential amino acids (NEAA), 2mM glutamine, and 100 units/mL penicillin and 100 µg/mL streptomycin at 37.0° Celsius (C)and 5.0% CO2. Media was changed every 2-3 days.

Creating Bptf KD Cell Lines

Mouse breast cancer (4T1) and melanoma (B16F10) cell lines were plated on 6-well plates and, upon reaching 30-50% confluence, transduced with retroviral shRNA (pSIREN Retro-Q, Clontech) targeting Bptf and containing puromycin resistance. Cells were incubated with retrovirus for 48 hours, then placed into media containing 5µg/mL puromycin (Gibco) for selection of cells successfully incorporating the desired shRNA. Cells surviving puromycin selection were split and either frozen or utilized for protein extraction. Bptf KD cell lines were confirmed via Western blot analysis off of 6 well plates, and again off of 10 cm plates to ensure KD consistency. Cell lines were then frozen down and stored in liquid nitrogen.

Creating OVA Cell Lines

Melanoma (B16F10) cells were plated and co-transfected with DNA for both the ovalbumin (ova) and zeocin resistance genes. Ovalbumin DNA received from the Wang lab was altered to remove the existing puromycin resistance gene. Cells were transfected with the ovalbumin and zeocin resistance DNA and Lipofectamine 2000 (Invitrogen) for 48 hours, then placed into media containing 0.2% zeocin (Invitrogen) over multiple weeks for selection of cells incorporating the desired segments. Single clones were isolated and screened for incorporation of ovalbumin by flow cytometry utilizing staining with OVA257-264 peptide bound to H-2Kb (BD Pharmingen) on the BD FACS Calibur Flow Cytometer. Two separate cell lines (out of 15 screened) incorporating ovalbumin were then utilized to create Bptf KD and control cell lines as described above. Both Bptf KD and ovalbumin expression were confirmed by Western blot analysis.

Solid Tumor Flow Cytometry

Spleens from Bptf KD and control tumor-bearing mice and tumors were extracted from mice and placed on ice. Tumors were weighed, then mechanically minced by razor blade in a petri dish. Tumors were subsequently digested in enzyme solution containing 1μg/mL Collagenase Type IV (Sigma) and 20 μg/mL DNase I (Sigma) in PBS (10mL of enzyme solution for tumors 1 cm^2 in size) for 90 minutes in a 37°C water bath. During the 90 minute incubation, digests were inverted every 15 minutes. Digests were then filtered through a 40 μm filter and centrifuged at 1500 rpm for 5 minutes at room temperature. After removal of the supernatant, cells were resuspended in 9 mL 40% Percoll (Sigma) diluted in PBS and carefully layered on top

of 4 mL of 70% percoll containing 10 µL 0.5% phenol red dye (Sigma) in PBS, creating a discontinuous gradient. Percoll gradients were centrifuged at 3000 x g for 30 minutes at room temperature with minimal acceleration and brake. Cells at the interface were collected and diluted with 30 mL PBS, then centrifuged at 1500 rpm for 5 minutes. Supernatant was removed, and cells were resuspended in 1 mL of cold FACS buffer. Cells were then counted in a 1:1 ratio of 0.2% trypan blue viability dye and split evenly into two tubes.

Spleens, utilized for compensation controls in addition to being samples, were placed on a petri dish in 1 mL cold FACS buffer and sliced in half lengthwise with a razor blade. Splenocytes were massaged out with the flat end of a sterile 5 mL syringe plunger and filtered through a 40 µm filter. Splenocytes were separated into multiple tubes for samples and controls and centrifuged at 500 g for 5 minutes at room temperature. Supernatants were removed and cells were resuspended in 500 µL RBC lysis buffer (155 mM NH_4CL, 12 mM $NaHCO_3$, 0.1 mM EDTA in molecular grade water). The RBC lysis reaction continued room temperature for 4-5 minutes and was stopped with 1 mL PBS. Splenocytes were centrifuged at 500 g for 5 minutes and resuspended in 1 mL cold FACS buffer (2% FBS in Hank's balanced salt solution (HBSS)).

All samples were stained with a combination of CD8 (FITC), TCRβ (PE), or CD69 (PE) antibodies (BD Pharmingen) for 20 minutes, shielded from light. Cells were washed twice in 1 mL cold FACS buffer and resuspended in 500µL FACS buffer containing 2 ng/mL 7AAD (Sigma) for analysis by flow cytometer (BD FACS Calibur Flow Cytometer). Flow cytometry data was analyzed using FlowJo software.

Cell Culture Flow Cytometry

Cells cultured to approximately 80% confluence were washed twice with 1X PBS and placed in 1 mL Cellstripper (Cellgro) solution at 37°C until single cell suspension was reached. Cells were then centrifuged at 350 g for 5 minutes, resuspended in 1 mL FACS buffer, and stained with OVA(257-264) peptide bound to H-2Kb (eBioscience, 12-5743-81) for 20 minutes, shielded from light. Cells were washed twice in 1 mL cold FACS buffer and resuspended in 500 µL cold FACS buffer for analysis by flow cytometer (BD FACS Calibur Flow Cytometer). Flow cytometry data was analyzed with FlowJo software.

ELISA

eBioscience ELISA Ready-Set-Go! protocol was followed as provided by the company. Briefly, 96-well plates were coated with capture antibody and incubated overnight at 4°C. Wells were washed with provided Wash Buffer, blocked for 1 hour at room temperature in diluted Assay Diluent, and then washed again. Standards and samples were added (100 µL/well) and incubated overnight at 4°C. Wells were washed the next morning, placed in primary (detection) antibody for 1 hour at room temperature, washed, placed in secondary (Avidin-HRP) antibody for 30 minutes at room temperature, and washed again. Finally, 100µL of Substrate Solution was added to each well for 15 minutes at room temperature before 50µL Stop Solution was added to each well and the plate was read at 450 nm and 570 nm by spectrophotometer (Synergy H1 Multi-Mode Plate Reader, BioTek).

LDH Cytotoxicity Assay

Promega CytoTox 96 Non-Radioactive Cytotoxicity Assay protocol was followed as provided by the company. Briefly, a 96-well plate was plated with 1,000 effector cells/well and incubated overnight at 37°C. The following morning, target cells were added to all experimental wells and appropriate control wells in pre-determined effector:target ratios, and the plate was centrifuged for 4 minutes at 250 g. The plate was then incubated at 37°C overnight, after which provided 10X Lysis Solution was added to appropriate. Supernatant (50µL) from each of the wells was then transferred to an enzymatic assay plate where 50 µL of Substrate Mix was added to each well. The enzymatic assay plate was covered and incubated for 30 minutes at room temperature, shielded from light. Finally, after the 30 minute incubation, 50 µL Stop Solution was added to each well and the absorbance was read at 490 nm by spectrophotometer (Synergy H1 Multi-Mode Plate Reader, BioTek).

Western Blot

Cultured cells were washed twice with PBS, then placed in 1 mL of TRI reagent (Sigma) and incubated at room temperature for 10 minutes. The 1 mL of TRI reagent was then forcefully pipetted over the cells multiple times to homogenize the extract. The sample was placed into a 1.5 mL centrifuge tube and 200 µL chloroform was added. Samples were vortexed for 15 seconds, allowed to sit at room temperature for 10-15 minutes, and centrifuged at 12,000 x g at 4°C for 15 minutes. The upper clear aqueous layer containing RNA and thin viscous interphase containing DNA were removed by vacuum and 1 mL isopropanol was added to the organic layer. The sample was inverted to mix and incubated at room temperature for 10 minutes while a while precipitate (protein) formed. Samples were then centrifuged at 12,000 x g at 4°C for 10 minutes and the supernatant was aspirated. To the protein pellet, 1.5 mL of 0.3 M guanidine in 95%

ethanol was added. The pellet was dislodged and the sample was placed on a rocker at 4°C overnight. The next day, samples were centrifuged at 12,000 x g at 4°C for 15 minutes. After aspiration of the supernatant, 1.5 mL 100% ethanol was added and incubated at room temperature for 20 minutes. Samples were subsequently vortexed and spun down at 12,000 x g at 4°C for 15 minutes and the supernatant was aspirated. To the pellet, 200 µL 8M urea in 1% SDS was added and samples were incubated at 65°C overnight. The following morning, protein was quantified for each sample against standards (0 mg/mL, 0.75 mg/mL, 1.5 mg/mL, and 3 mg/mL all in BSA) using BioRad DC Protein Assay reagents, incubated at room temperature for at least 10 minutes, and absorbance was measured at 750 nm by spectrophotometer (Pharmacia LKB Ultrospec III). 5X SDS loading buffer and 8M urea in 1% SDS were added to bring each sample to a protein concentration of 2 mg/mL.

Cell protein extracts (40µg) were then run on a 4%, 6%, 10%, or 15% Tris/Glycine gel (depending on protein size) for 1 hour at 200 V and 200 mA. Protein extracts were then transferred to Immuno-Blot polyvinylidene difluoride (PVDF) membrane (Bio-Rad) by Western blot in either CAPS buffer (10 mM CAPS pH 10.5, 00025% 1 M DTT in diH2O) or 1X Tris/Glycine transfer buffer (25 mM Tris, 190 mM Glycine) for 17 hours at 20 V and 20 mA. Membranes were removed and blocked in 5% NFDM in PBST (PBS, 0.001% Tween-20) for 1 hour, then placed in 10 mL 5% NFDM in PBST and primary antibody and incubated on an orbital shaker overnight at 4°C. Primary antibody concentrations added were as follows: 3 µL α-Bptf (Landry), 10 µL α-Ovalbumin (Santa Cruz Biotechnology, 3G2E1D9), or 10 µL Pmel17 (Santa Cruz Biotechnology, H-300) per membrane. After incubation in primary antibody, membranes were rinsed with PBST 3 times for 7 minutes each, and blocked in 10 mL 5% NFDM in PBST and secondary antibody for 1 hour. Secondary antibody concentrations added were as

follows: 1μL anti-mouse IgG (Cell Signaling Technology, #7076), or 1 μL anti-rabbit IgG (Cell Signaling Technology, #7074). Membranes were then rinsed again in PBST 3 times for 7 minutes each. Membranes were bathed in 500 μL ECL (Thermo Scientific SuperSignal West Femto), wrapped in a single layer of cling wrap and placed on x-ray film for varying lengths of time. Films were developed using an automated tabletop processor.

Quantitative Western Blot

Cell protein extracts (40μg) were run on a 6%, 10%, or 15% Tris-Glycine gel for 1 hour at 200 V and 200 mA. Protein extracts were then transferred to Immuno-Blot PVDF membrane (Bio-Rad) by Western blot in CAPS buffer or Tris/Glycine transfer buffer for 17 hours at 20 V and 20 mA. Membranes were removed and blocked in 5% NDFM in PBST for 1 hour, then placed in 10 mL 5% NFDM in PBST and primary antibody and incubated on an orbital shaker overnight at 4°C. Primary antibody concentrations added were as follows: 3 μL α-Bptf (Landry), 10 μL α-Ovalbumin (Santa Cruz Biotechnology, 3G2E1D9), 10 μL Pmel17 (Santa Cruz Biotechnology, H-300), or 1 μL cyclophilin B (abcam, ab3565) per membrane. After incubation in primary antibody, membranes were rinsed with PBST 3 times for 7 minutes each, and blocked in 10 mL 5% NFDM in PBST and secondary antibody for 1 hour. Secondary antibody concentrations added were as follows: 1 μL anti-mouse IgG (Cell Signaling Technology, #7076), or 1 μL anti-rabbit IgG (Cell Signaling Technology, #7074). Membranes were bathed in 500 μL ECL (Thermo Scientific SuperSignal West Femto) and placed on the provided tray and inserted into the Odyssey Fc (LI-COR) imaging system for quantitative image capture and analysis.

RESULTS

Bptf KD Tumors Display an Elevated CD8 T Cell Population

It was previously observed through systematic depletion of immune cells that CD8 cells are an essential part of the mechanism involved in the phenotypic difference seen between control and Bptf KD tumors. Prior experiments also revealed that CD8 T cells primed on Bptf KD cells kill Bptf KD cells more effectively than T cell primed on control cells kill control cells *in vitro*. To determine whether the mechanism behind the increased cytotoxicity of Bptf KD T cells was due to an increase in activated CD8 T cells in Bptf KD tumors, flow cytometry was performed on Bptf KD and control solid tumors obtained the same day.

The presence of tumor infiltrating CD8 cells was evaluated by staining cells for both CD8 and TCRb in both 4T1 and B16F10 control and Bptf KD tumors. A stepwise gating strategy (Figure 10). First, the lymphocyte population was isolated, then gating specifically on live cells, and finally gating on the CD8 positive population within the TCRb population was employed. Percentages, as opposed to cell counts, were utilized to account for the difference in tumor weight as well as variability in cell counts between samples of the same tumor, and to enable direct comparisons between tumors.

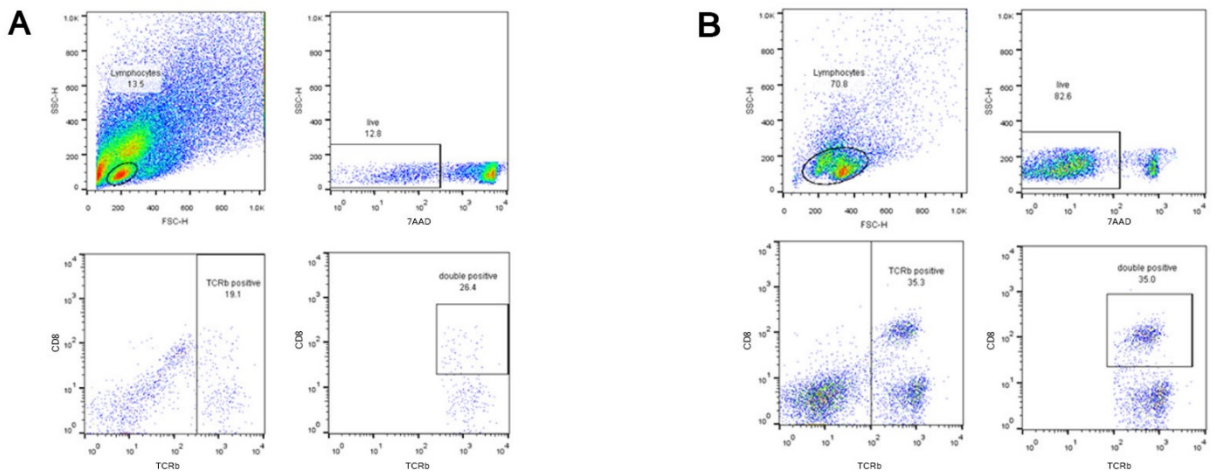

Figure 10: Gating Strategy for Determining CD8 Populations. (A) Gating strategy utilized in tumors. The lymphocytes population was first gated off of, followed by the live population of lymphocytes. TCRb+ cells were then gated out of the live population, and of that population, CD8+ (double positive for TCRb and CD8) T cells were determined. (B) The same gating strategy as described in A shown for spleens.

The T cell population was considered to be all cells staining positive for TCRβ, after isolation of live lymphocytes. Exact gating strategies employed for extraction of the CD8 cell population in tumors and spleens are illustrated in Figure 10.

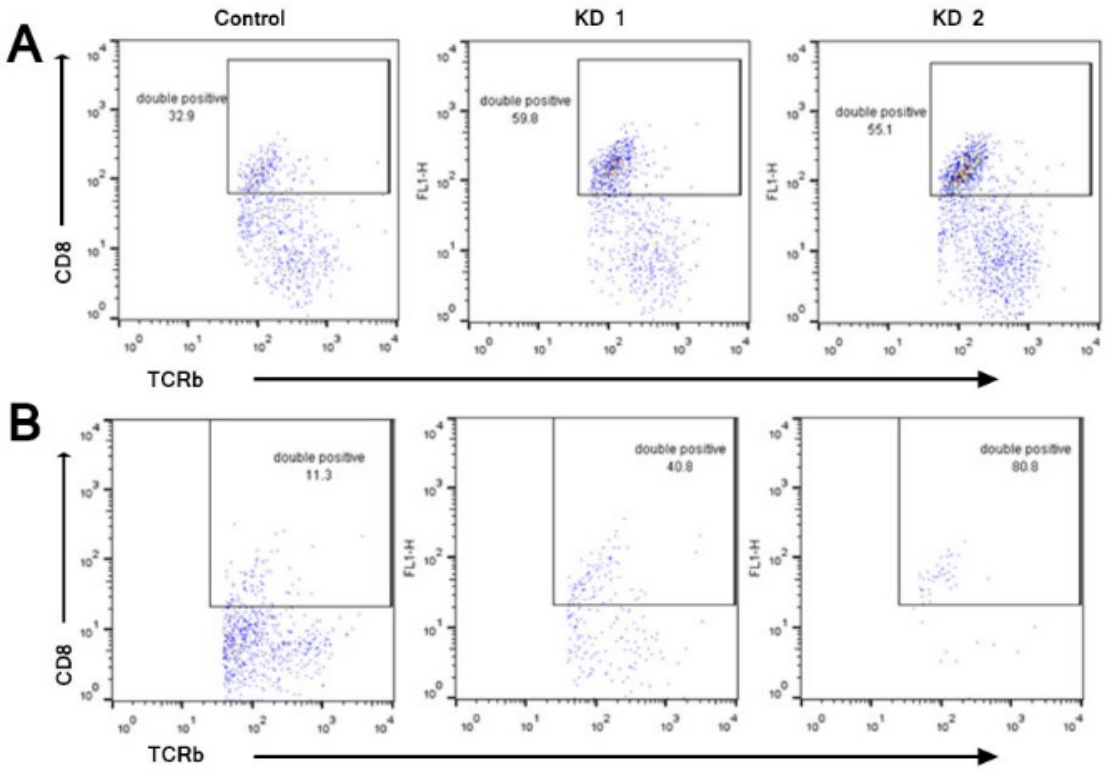

Figure 11: CD8+ T Cell Population in 4T1 and B16F10 Tumors. Dot plots showing TCRb+/CD8+ cells in a single tumor for control and Bptf KDs in 4T1 (A) and B16F10 (B) tumors.

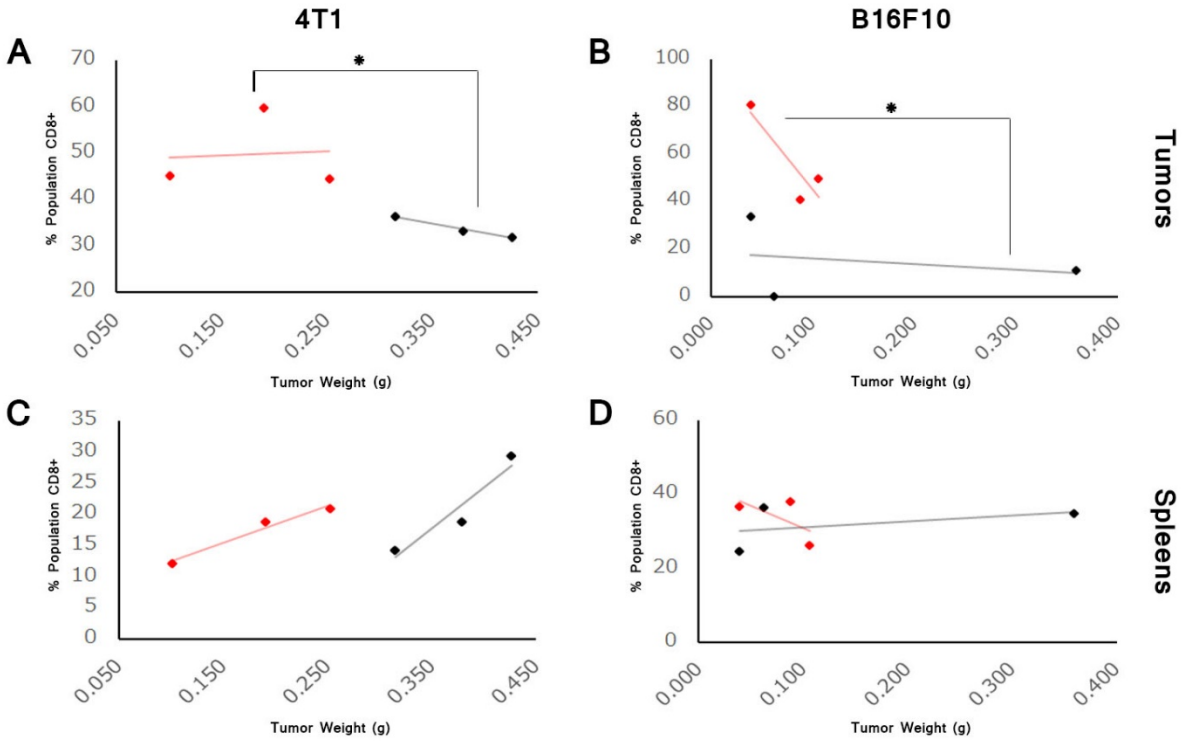

Figure 12: CD8+ T Cell Population in Tumors and Spleens. Representative Bptf KD (red) and control (black) CD8+ populations by tumor weight showing a significant difference between Bptf KD and control tumor CD8+ populations in 4T1 (A) and B16F10 (B) tumors. Similar analysis of CD8+ populations in spleens by tumor weight in both 4T1 (C) and B16F10 (D) mice showing no significant difference.

Dot plots for the percentage of CD8+ T cells in single 4T1 and B16F10 control, Bptf KD 1, and Bptf KD 2 tumors are provided in Figure 11. Analysis of the microenvironment of multiple tumors derived from both the 4T1 and B16F10 cell lines showed significant differences in CD8+ T cell populations between control to Bptf KD tumors. There were significantly more CD8+ T cells in Bptf KD tumors as compared to control tumors for both 4T1 (p-value = 0.03) and B16F10 (p-value = 0.05), as shown in Figure 12. Trends between CD8+ T cell levels and tumor weights were also visualized. As tumor weight decreased, the presence of CD8+ cells increased in both 4T1 (Figure 12A) and B16F10 tumors (Figure 12B). In splenocytes from 4T1

and B16F10 tumor-bearing mice, however, the opposite trend was shown in all but one population. For spleens from 4T1 control, Bptf KD (Figure 12C), and B16F10 control tumor-bearing mice (Figure 12D), as tumor weight increased, the percentage of CD8+ splenocytes also increased. Conversely, in splenocytes from B16F10 Bptf KD tumor-bearing mice, it was seen that the CD8+ population decreases with increasing tumor weight (Figure 12D).

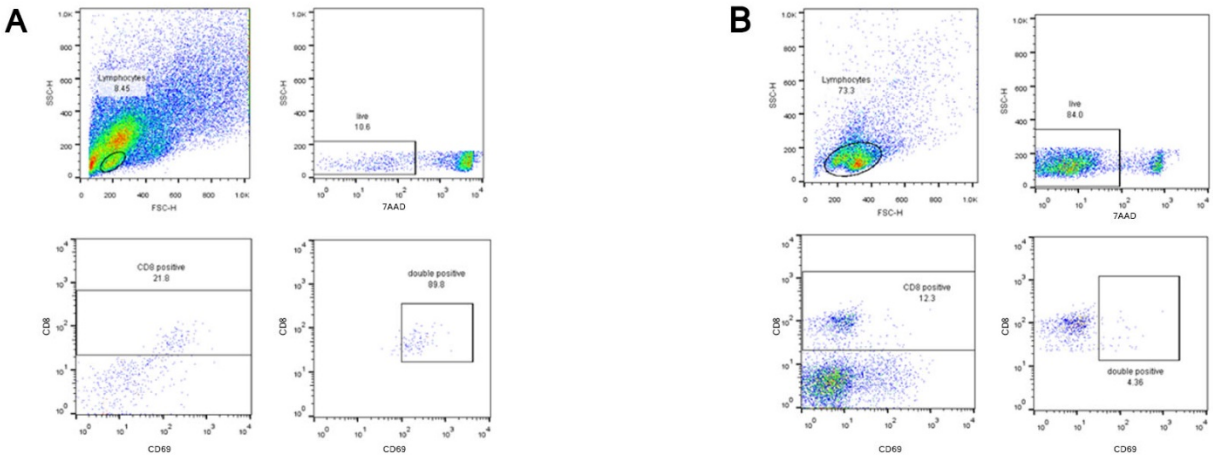

Figure 13: Gating Strategy for Determining Active CD8 Populations. (A) Gating strategy utilized in tumors. The lymphocytes population was first gated off of, followed by the live population of lymphocytes. CD8+ cells were then gated out of the live population, and of that population, CD69+ (double positive for CD8 and CD69) T cells were determined. (B) The same gating strategy as described in A shown for spleens.

Tumors derived from 4T1 and B16F10 cell lines were also analyzed for CD8 T cell activation status. Exact gating strategies employed for determination of the active CD8 population in tumors and spleens are illustrated in Figure 13. Dot plots for active (CD69+) CD8+ T cell determination in single 4T1 and B16F10 control, Bptf KD 1, and Bptf KD 2 tumors are provided in Figure 14. While significant differences in active CD8+ T cell populations were not observed between control to Bptf KD tumors, a clear trend was again visualized. As tumor weight decreased, the presence of active CD8+ cells in the tumor microenvironment increased in

4T1 Bptf KD and control tumors (Figure 15A), as well as B16F10 Bptf KD tumors (Figure 15B). The microenvironment of B16F10 control tumors showed an opposing correlation, with active CD8 cell status increasing with increasing tumor weight (Figure 15B). Analysis was also performed on the spleens of 4T1 and B16F10 Bptf KD and control tumor-bearing mice. No significant differences were observed between control and Bptf KD groups, however a similar trend was detected. In splenocytes from 4T1 Bptf KD or control tumor-bearing mice (Figure 15C) or B16F10 control tumor-bearing mice (Figure15D), activation status of CD8 cells decreased as tumor weight increased. The activation status of CD8 cells in splenocytes from B16F10 Bptf KD tumor-bearing mice did not follow this trend as definitively as other groups (Figure 15D).

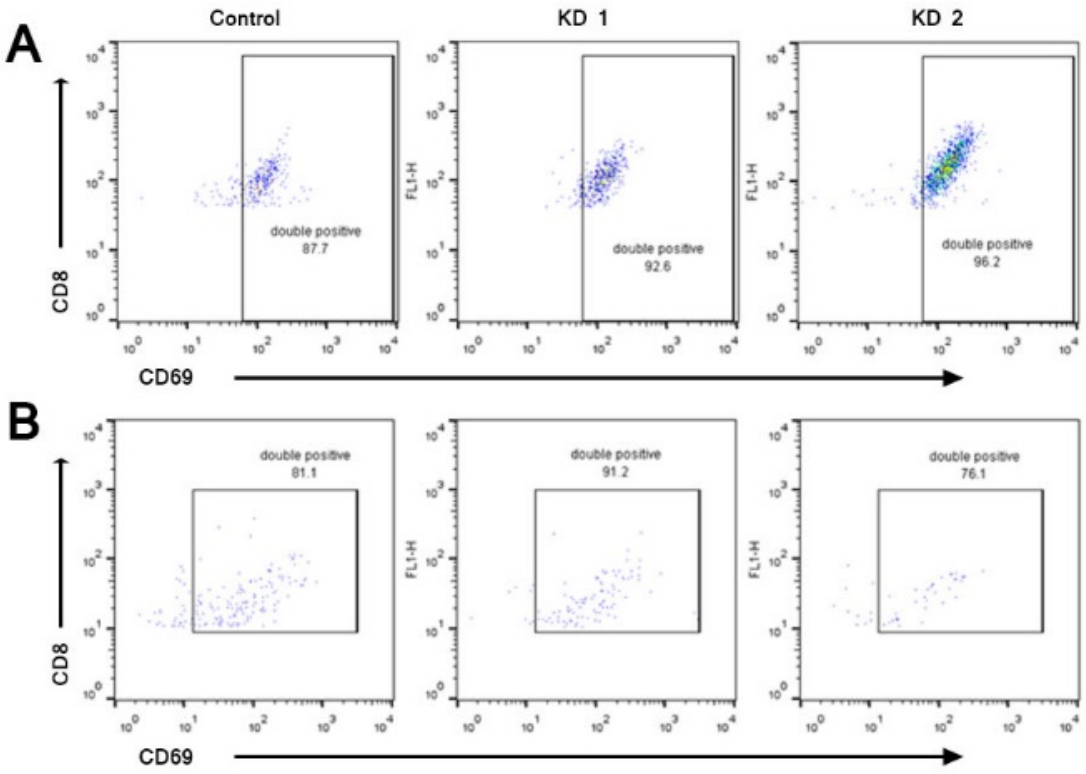

Figure 14: Active CD8 T Cell Population in 4T1 and B16F10 Tumors. Dot plots showing CD8+/CD69+ cells in a single tumor for control and Bptf KDs in 4T1 (A) and B16F10 (B) tumors.

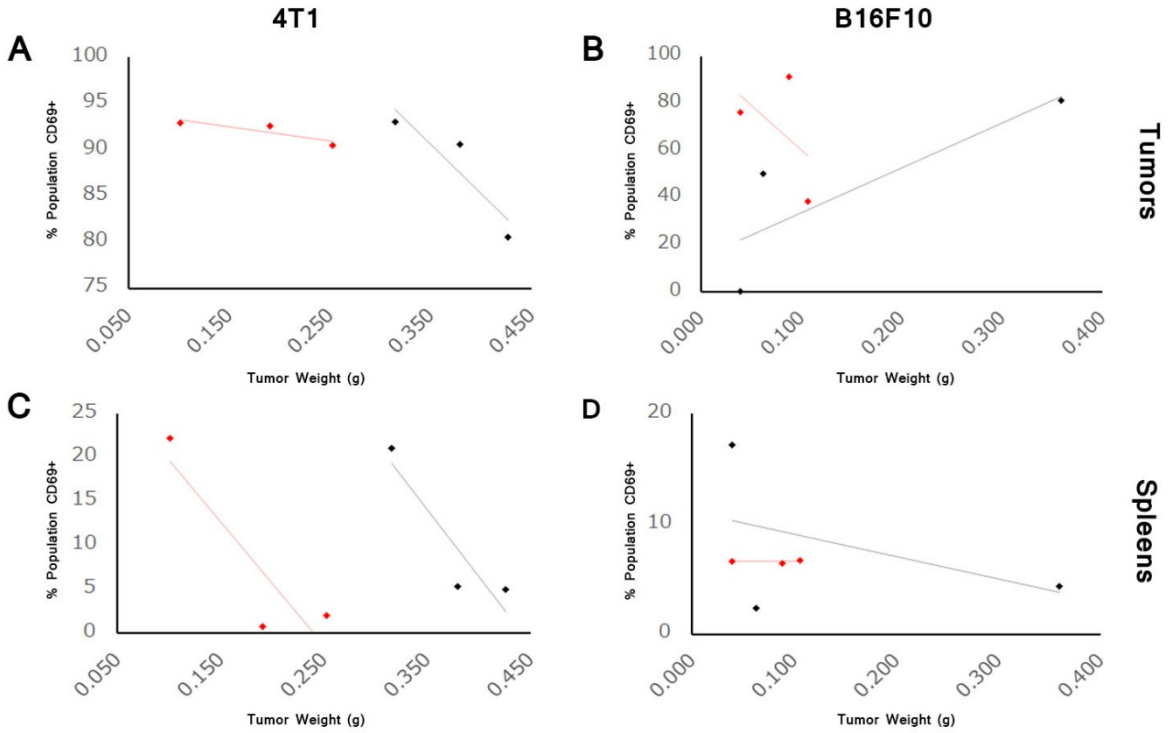

Figure 15: Active CD8 Population Decreases with Increasing Tumor Weight.
(A) Representative Bptf KD (red) and control (black) CD69+ populations by tumor weight illustrating the trend that as tumor weight decreases, presence of CD69+ CD8 T cells increases in Bptf KD and control 4T1 tumors. (B) Similar analysis of B16F10 Bptf KD and control tumors. Similar analysis of CD8+ populations in spleens by tumor weight in both 4T1 (C) and B16F10 (D) mice showing a decrease in CD69+ population as tumor size increases.

Bptf KD Tumors do not Present OVA or Pmel-17 Antigen with Greater Efficiency

Previous data gathered or provided evidence for the upregulation of genes involved in MHC Class I antigen processing. Additional experimental data went on to illustrate no significant increase in the overall presence of MHC Class I molecules on the cell surface. With this information, we set out to determine if Bptf KD cells alter antigen presentation. Specifically, we wanted to extrapolate whether antigen is presented with greater efficiency on the surface of Bptf KD tumor cells as compared to control tumor cells.To determine if Bptf KD tumors present

antigen in greater amounts on the cell surface, two separate model systems utilizing known antigen were evaluated.

OT1 Model

The OT-1 model is well characterized and frequently used for investigation into antigen presentation and CD8 T cell responses to antigen [53,54,55,56]. OT-1 mice are C57BL/6 mice transgenic for the OT-1 T-cell receptor, producing CD8 T cells that are MHC class I restricted and ovalbumin (257-264) specific [57]. OVA, the gene encoding for the hen egg protein ovalbumin, is not native to the B16F10 cell line. With previous data showing KD of Bptf results in dysregulation of MHC Class I associated genes, dysregulation of genes associated with antigen processing for MHC Class I molecules, and the importance of CD8+ T cells in the mechanism used in Bptf KD tumors, use of the OT-1 model (with a known non-native antigen specific for MHC Class I that utilizes restricted CD8+ T cells) was chosen. Once incorporated into the desired cell line(s), presentation of OVA (257-264) in the context of MHC Class I haplotype H2-Kb can be evaluated to determine antigen presentation efficiency and CD8 T cell cytotoxicity.

The ovalbumin (OVA) gene was introduced into B16F10 cells to create the parents cell lines used for this model. Flow cytometry of the lines was utilized to confirm expression of OVA on the cell surface (Figure 16).

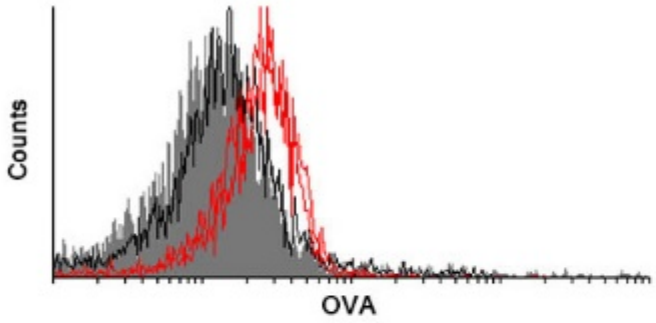

Figure 16: Confirmation of Ovalbumin Gene Incorporation and Expression in B16F10 Cell Lines. Expression of OVA(257-264) complexed with H2-Kb on B16F10 cells. Isotype (gray), B16F10 control without OVA (black), two B16F10 lines transfected with OVA (red).

Bptf KD lines were created from the B16F10 clones incorporating the OVA gene, and expression of both OVA and Bptf were confirmed via Western blot (Figure 17A). Cell lines were then evaluated for OVA expression by quantitative Western blot and flow cytometry. For quantitative western blot data analysis, OVA expression was determined as the ratio of OVA expression to that of cyclophilin B as loading control for each sample. Analysis revealed no significant difference in OVA expression from control to Bptf KD lines (Figure 17B).

OVA expression of Bptf control and KD cell lines was also evaluated by flow cytometry. The OVA antibody used for flow cytometry analysis was for OVA(257-264) peptide complexed with the H2-Kb molecule. Analysis of both MHC Class I molecule H2-Kb and OVA expression revealed a slight increase in H2-Kb expression in Bptf KD cell lines, but no discernable difference in cell surface OVA expression levels (Figure 17D). Analysis of H2-Kb alone ensured any observed change in OVA expression localized to the cell surface was not due to an increase in cell surface MHC Class I H2-Kb. Mean fluorescence intensity (MFI) of both H2-Kb and OVA were also calculated from flow cytometry data. OVA expression for control and Bptf KD cell

lines was calculated as a ratio of OVA MFI to H2-Kb MFI. This analysis revealed a visible but insignificant decrease of cell surface OVA expression in Bptf KD cells (Figure 17C).

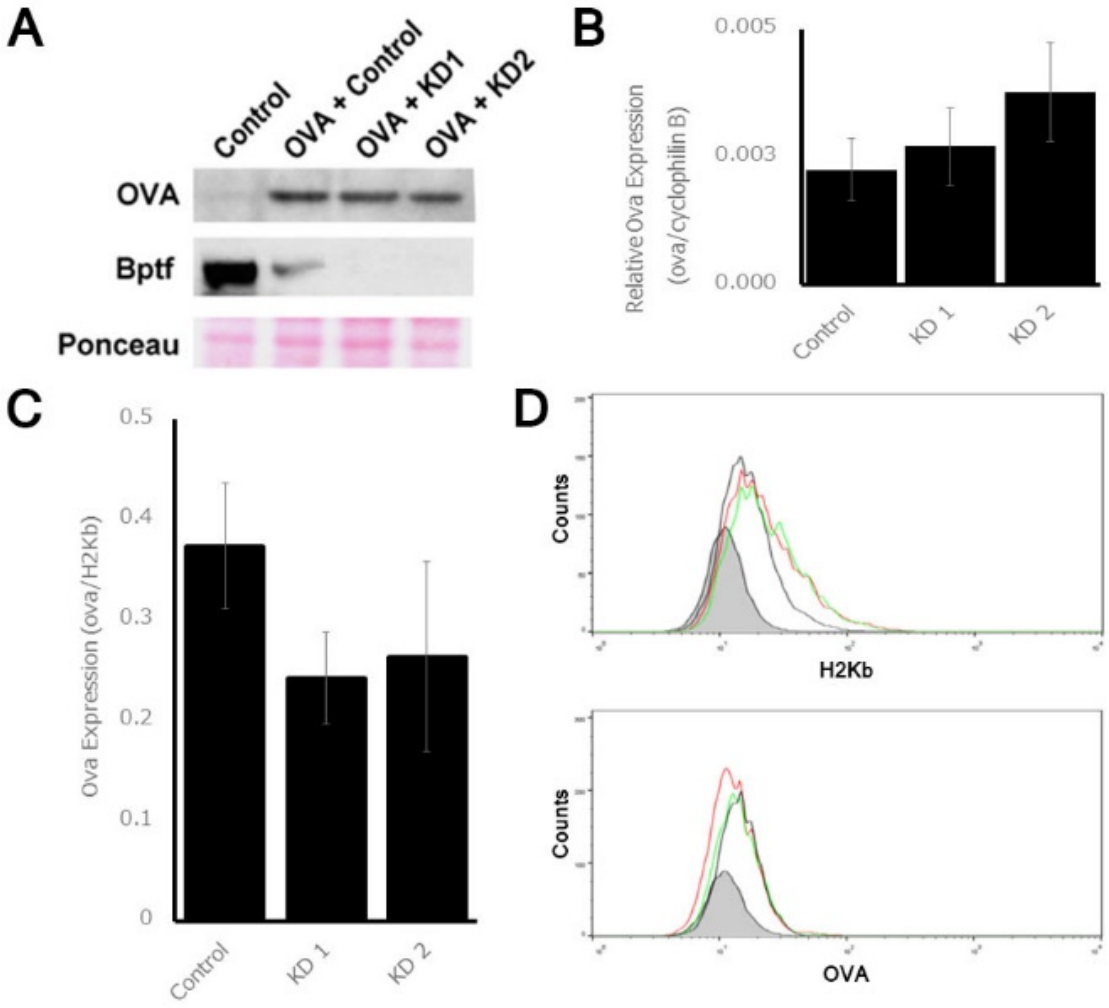

Figure 17: Relative OVA Expression of Bptf Control and KD Cell Lines as Determined by Flow Cytometry Analysis. (A) Western blot analysis confirming ova expression in OVA cell lines and not control. Bptf KD was also confirmed, with B16F10+OVA lines with Bptf KD showing no expression of Bptf compared to controls. Ponceau staining provided as loading control. (B) Quantitative Western blot analysis of OVA expression shown as a ratio of OVA expression to the loading control cyclophilin B. (C) MFI of OVA expression as a ratio of OVA to H2-Kb in control and Bptf KD B16F10+ova cells, determined by flow cytometry. (D) Flow cytometry of H2-Kb and OVA expression in B16F10+ova Bptf KD and control cell lines. Isotype (gray), B16F10+OVA control (black), B16F10:OVA Bptf KDs (red and green).

T cells obtained from an OT-1 mouse were then placed onto B16F10+OVA control and Bptf KD cell lines to determine cell death *in vitro*. A preliminary LDH cytotoxicity assay performed revealed no significant difference in cell death from B16F10+OVA control to Bptf KD cell lines (Figure 18).

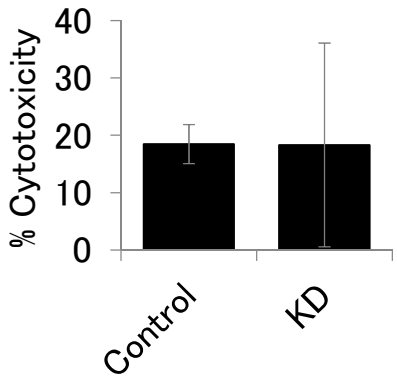

Figure 18: LDH Cytotoxicity of Bptf Control and KD OVA-Expressing T Cells. No significant difference was revealed between control and Bptf KD B16F10+OVA cells concerning cell death efficiency as determined by preliminary LDH cytotoxicity assay.

Pmel-17 Model

A second model used focused on presentation of a known native antigen, as opposed to the non-native antigen introduced through the OT-1 model. The Pmel-17 model focuses on the presentation of the naturally expressed Pmel-17 antigen in C57BL/6 mice. Pmel-17 is a naturally expressed antigen found on both normal melanocytes, as well as a large portion of malignant melanomas in humans [58,59]. Analysis of the expression of pmel-17 on B16F10 control and Bptf KD cell lines will allow examination of antigen presentation efficiency and cytotoxicity in the same manner as the OT-1 model, but provide insight into the antigen presentation status of native antigens.

Expression of Pmel-17 and Bptf were confirmed in existing control and Bptf KD B16F10 cell lines by Western blot (Figure 19). These cell lines were then evaluated for expression of Pmel-17 by Western blot analysis (Figure 19).

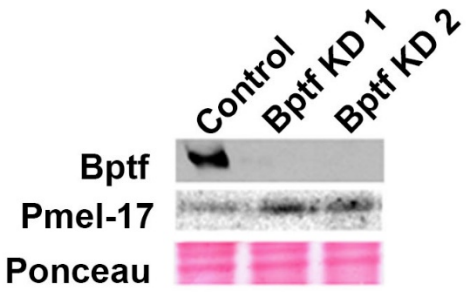

Figure 19: Stable Bptf KD and Pmel-17 Expression of B16F10 Cell Lines. Western blot analysis confirming expression of Pmel-17 and appropriate levels of Bptf in control and Bptf KD B16F10 cells. Ponceau staining provided as loading control.

T cells obtained from a Pmel-17 mouse were then placed onto B16F10 control and Bptf KD cell lines to determine cytotoxicity and cell death *in vitro*. Preliminary LDH cytotoxicity assays revealed a decrease in cytotoxic effect of T cells to Bptf KD tumor cell targets as compared to control tumor cell targets (Figure 20A). Preliminary analysis of cell death by ELISA was also performed, showing evidence in concurrence with LDH cytotoxicity assay results. Figure 20B illustrates the decrease in IFN-γ release induced by Pmel-17 T cells placed on Bptf KD tumor cell targets as compared to Pmel-17 T cells placed on control tumor cell targets seen through IFN-γ ELISA analysis.

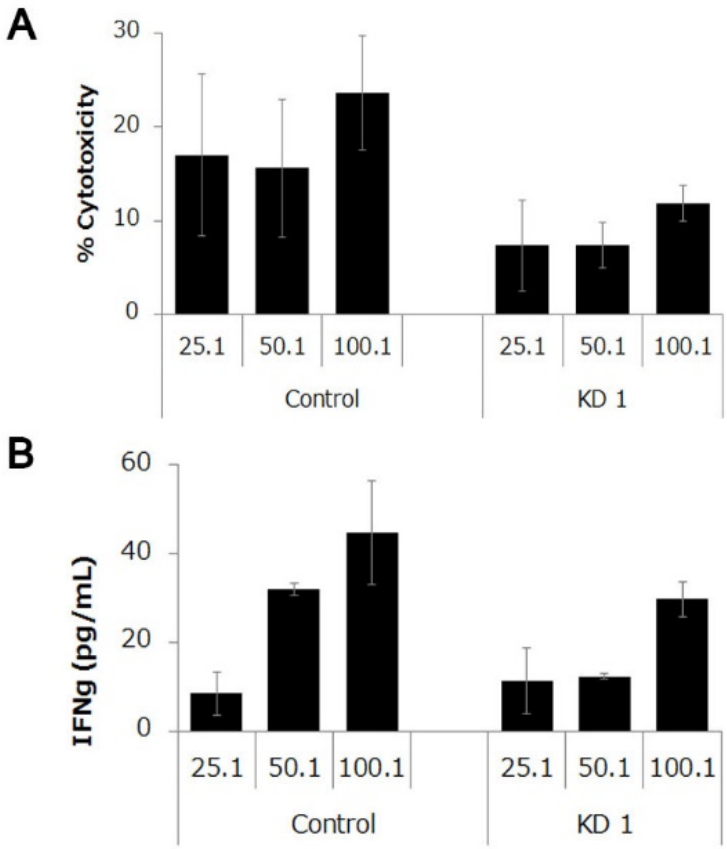

Figure 20: LDH Cytotoxicity of Pmel-17 T Cells Similar on Bptf Control and KD Cell Lines. Preliminary LDH cytotoxicity assay (A) and IFN-γ ELISA (B) results showing a decrease in cell death of Bptf KD cells by Pmel-17 sensitive CD8+ T cells.

DISCUSSION

While advances in cancer treatment have been made over the past 25 years, 1 in 4 deaths in the United States continues to be attributed to cancer [1]. Of the treatments available, immunotherapies are relatively recent and have gained notoriety with their ability to mitigate diseases that previously had a grim outlook and little to no available therapy, including cancer. Even with great strides being made in immunotherapies, epigenetics is an avenue of immunotherapy yet to be fully exploited for its therapeutic possibilities.

Through studies of the Bptf subunit, the chromatin remodeler NURF presents itself as a potential therapeutic target, with prior research demonstrating its necessity for embryonic development through Bptf KO cells, but also showing Bptf is not cell essential through use of cell-type specific Bptf KO studies [15,16]. Previous data revealing a decrease in tumor weights when Bptf is knocked-down heighten its therapeutic possibilities. With data indicating Bptf acts through manipulation of the immune system, Bptf begins to present itself as a target for future immunotherapies.

While Bptf is a likely candidate for immunotherapies, further investigation into the particular mechanism by which Bptf acts on the immune system will present even greater therapeutic possibilities. Once a mechanism is elucidated, manipulation of multiple portions of said mechanism could provide a variety of different clinically relevant areas of attack in the battle against cancer.

To begin to illuminate the mechanism by which Bptf decreases tumor weight, we examined the microenvironment of the tumor itself utilizing flow cytometry of two separate cell lines: 4T1 and B16F10. After digestion of the tumor and isolation of lymphocytes, cells were stained with a combination of antibodies for TCRβ, CD8, CD69. From a combination of these stains, we were able to determine the percentage of live CD8 cells present in the tumor microenvironment, as well as the percentage of live active CD8 cells present.

A total of 6 representative 4T1 tumors (3 control and 3 Bptf KD) and 6 melanomas (3 control and 3 Bptf KD) derived from the B16F10 cell line in addition to spleens from tumor-bearing mice were obtained and analyzed by flow cytometry for this project. In 4T1 and B16F10, we observed a significant increase in the percentage of CD8+ T cells in Bptf KD tumors as compared to controls. While no significant differences were realized in other relationships, multiple trends developed, including that of an increase in active CD8 T cells as tumor weight decreased. These insignificant differences may be realized as significant with additional data collection and analysis, due to time restrictions associated with this project.

From currently available data, there is an elevation of CD8+ T cells in the Bptf KD tumor microenvironment of both 4T1 and B16F10 cell line origin as compared to control. At this time, it is likely beneficial to reserve judgement on data obtained from B16F10 tumors, as they did not provide consistent results and analysis was based on a low number of available T cells. B16F10 tumors are known to harbor fewer T cells than other cancer cell lines [60]. This could not only make the recovery of T cells more difficult, but could contribute to any insignificance of data gathered, as greater cell counts contribute to more consistent and more reliable data analysis. With further adjustments made on the protocol utilized to obtain lymphocytes, including compilation of multiple control or Bptf KD tumors into one sample, elevated and consistent T

cell counts could be obtained. Once consistent results are obtained, more weight would be given to B16F10 data. At this time, a higher level of confidence is had in the data obtained from 4T1 tumors, which provided a more reasonable number of T cells for analysis.

CD8+ cells are activated once they recognize and come in contact with the antigen:MHC Class I complex on a cell [28]. In the immunological environment of a tumor, CD8+ cells can be presented with novel antigens or native antigens. Analysis of CD8 T cell activation status in the tumor microenvironment by flow cytometry showed that as tumor weight decreased, active CD8 T cell population increased. To explain a more active CD8+ T cell phenotype seen in Bptf KD tumors, CD8+ cells are likely either presented with novel antigens from the tumor, or tumors are exhibiting increased presentation of native antigens. Novel antigen presentation could attract more attention from the immune system and increase the activation of CD8+ cells, likely increasing cell death and providing definitive therapeutic potential. An increase in the efficiency of antigen presentation would provide more opportunities for recognition by cytotoxic CD8+ cells and therefore an increased chance of tumor cell death by CD8 cytotoxicity mechanisms, but provide a less clear-cut therapeutic opportunity.

While ongoing studies in the Landry Lab are investigating the possibility that Bptf KD tumor cells display novel antigens, the studies contained in this project explore the concept of increased antigen presentation occurring on Bptf KD tumor cells. Two separate models with known antigens were utilized for analysis of antigen presentation efficiency.

After we incorporated the ovalbumin gene into B16F10 cell lines for use of the OT-1 model, and subsequently introduced control or Bptf KD shRNA, we began analyses. OVA expression was consistently shown to have no significant difference in expression from control to Bptf KD cell lines. With no significant difference in presentation of the OVA antigen on the

cell surface, it was anticipated that no difference in cell death would be seen between OVA-expressing control and Bptf KD cells when exposed to CD8+ cells restricted to OVA. For use of the Pmel-17 model, CD8+ T cells were purified from the spleen of a Pmel-17 mouse and assays investigating cell death began. Cell death was measured through LDH cytotoxicity assay and/or IFN-γ ELISA. Only preliminary data for both the OT-1 and Pmel-17 models was obtained for this project. Initial data obtained by LDH cytotoxicity assay for the OT-1 model showed no significant difference between B16F10+OVA control and Bptf KD cell lines. Preliminary LDH cytotoxicity assay data for Pmel-17 showed a decrease in Bptf KD cell death when exposed to T cells from a Pmel-17 mouse as compared to controls. Preliminary IFN-γ ELISA data for Pmel-17 showed a decrease in IFN-γ production in wells containing Pmel-17 CD8 T cells placed on Bptf KD tumor cells as compared to wells with T cells placed on control tumor cells.

From data gathered during this project, the possible mechanisms behind decreased tumor weights in Bptf KD tumors begin to be narrowed down. IFN-γ and LDH cytotoxicity assays of both the OT-1 and Pmel-17 models, in combination with flow cytometry and quantitative Western blot analysis, reveal Bptf KD cells are likely not presenting antigen more efficiently on tumor cell membranes. These results support the model of a novel or tumor-associated antigen being presented on the surface of tumor cells. Flow cytometry of control and Bptf KD tumor microenvironments revealed Bptf KD tumors have an increased presence of CD8+ T cells that likely have an increased activation status as compared to controls. While much additional information must be gathered before making definitive conclusions, it is possible that Bptf KD tumor cells are presenting an antigen not normally expressed on that cell type/stage, resulting in an increase CD8+ and active CD8+ cell presence and increased tumor cell death by direct CD8 cytotoxicity mechanisms. These direct cytotoxicity mechanism could include release of perforin

and granzyme, release of IFN-γ and subsequent induction of the JAK/STAT pathway, or induction of the Fas/TRAIL pathway.

As stated previously, there are multiple limitations of this study. When use of tumors obtained the same day is required in any experiment, troubleshooting can be a significant source of delay, as we must have mice readily available for injection of cells that will take weeks to form tumors. If additional control and Bptf KD tumors are able to be gathered and analyzed, more distinct trends may be elicited. In regards to flow cytometry analysis of T cells obtained from B16F10 tumors, the minimal recovery of T cells may hinder the consistency of data obtained, requiring additional replicates to be completed for accurate results. Due to time restraints, all LDH cytotoxicity assay and ELISA data is to be considered preliminary, with replicates to be completed in the future for confirmation of results.

LITERATURE CITED

[1] Jemal A, Siegel R, Ward E, Hao Y, Xu J, Murray T, Thun MJ (2008). Cancer statistics, 2008. *CA Cancer J Clin* 58(2):71-96.

[2] Galluzzi L, Vacchelli E, Bravo-San Pedro JM, Buqué A, Senovilla L, Baracco EE, Bloy N, Castoldi F, Abastado JP, Agostinis P, Apte RN, Aranda F, Ayyoub M, Beckhove P, Blay JY, Bracci L, Caignard A, Castelli C, Cavallo F, Celis E, Cerundolo V, Clayton A, Colombo MP, Coussens L, Dhodapkar MV, Eggermont AM, Fearon DT, Fridman WH, Fučíková J, Gabrilovich DI, Galon J, Garg A, Ghiringhelli F, Giaccone G, Gilboa E, Gnjatic S, Hoos A, Hosmalin A, Jäger D, Kalinski P, Kärre K, Kepp O, Kiessling R, Kirkwood JM, Klein E, Knuth A, Lewis CE, Liblau R, Lotze MT, Lugli E, Mach JP, Mattei F, Mavilio D, Melero I, Melief CJ, Mittendorf EA, Moretta L, Odunsi A, Okada H, Palucka AK, Peter ME, Pienta KJ, Porgador A, Prendergast GC, Rabinovich GA, Restifo NP, Rizvi N, Sautès-Fridman C, Schreiber H, Seliger B, Shiku H, Silva-Santos B, Smyth MJ, Speiser DE, Spisek R, Srivastava PK, Talmadge JE, Tartour E, Van Der Burg SH, Van Den Eynde BJ, Vile R, Wagner H, Weber JS, Whiteside TL, Wolchok JD, Zitvogel L, Zou W, Kroemer G (2014). Classification of current anticancer immunotherapies. *Oncotarget* 5(24):12472-508.

[3] Weiner LM, Surana R, Wang S (2010). Monoclonal antibodies: versatile platforms for cancer immunotherapy. *Nat Rev Immunol* 10(5):317-327.

[4] Humphries C (2013). Adoptive cell therapy: honing that killer instinct. *Nature* 504(7480):S13-15.

[5] Sim GC, Martin-Orozco N, Jin L, Yang Y, Wu S, Washington E, Sanders D, Lacey C, Wang Y, Vence L, Hwu P, Radvanyi L (2014). IL-2 therapy promotes suppressive ICOD+ Treg expansion in melanoma patients. *J Clin Invest* 124(1):99-110.

[6] Melero I, Grimaldi AM, Perez-Gracia JL, Ascierto PA (2013). Clinical development of immunostimulatory monoclonal antibodies and opportunities for combination. *Clin Cancer Res* 19(5):997-1008.

[7] Maresca TJ, Heald R (2006). The Long and the Short of It: Linker Histone H1 is Required for Metaphase Chromosome Compaction. *Cell Cycle* 5(6):589-591.

[8] Alkhatib SG, Landry JW (2011). The Nucleosome Remodeling Factor. *FEBS Letters* 585:3197-3207.

[9] Meshorer E, Plath K (2010). *The Cell Biology of Stem Cells*. 1st Edition. New York: Landes Bioscience, Springer Science+Business Media, LLC.

[10] Németh A, Längst G (2003). Chromatin higher order structure: Opening up chromatin for transcription. *Brief Funct Genomic Proteomic* 2(4):334-343.

[11] Schwanbeck R, Xiao H, Wu C (2004). Spatial contacts and nucleosome step movements induced by the NURF chromatin remodeling complex. *J. Biol Chem* 279(38):39933-39941.

[12] Hamiche A, Sandaltzopolous R, Gdula DA, Wu C (1999). ATP-dependent histone octamer sliding mediated by the chromatin remodeling complex NURF. *Cell* 97(7):833-842.

[13] Flaus A, Owen-Hughes T (2003). Dynamic properties of nucleosomes during thermal and ATP-driven mobilization. *Mol Cell Biol* 23(21):7767-7779.

[14] Georgel PT, Tsukiyama T, Wu C (1997). Role of histone tails in nucleosome remodeling by Drosophila NURF. *EMBO J* 16(15):1406-1413.

[15] Landry JW, Sharov AA, Piao Y, Sharova LV, Xiao H, Southon E, Matta J, Tessarolo L, Zhang YE, Ko MSH, Kuehn MR, Yamaguchi TP, Wu C (2008). Essential role of chromatin remodeling protein Bptf in early mouse embryos and embryonic stem cells. *PLoS Genet* 4(10):e1000421.

[16] Landry JW, Banerjee S, Taylor B, Aplan PD, Singer A, Wu C (2010). Chromatin remodeling complex NURF regulates thymocyte maturation. *Genes & Development* 25:275-286.

[17] Sun J, Purcell L, Gao Z, Isaacs SD, Wiley KE, Hsu FC, Liu W, Duggan D, Carpten JD, Grönberg H, Xu J, Chang BL, Partin AW, Walsh PC, Isaacs WB, Zheng SL (2008). Association between sequence variants at 17q12 and 17q24.3 and prostate cancer risk in European and African Americans. *Prostate* 68(7):691-697.

[18] Choi JS, Zheng LT, Ha E, Lim YJ, Wang YP, Lim Y (2006). Comparative genomic hybridization array analysis and real-time PCR reveals genomic copy number alteration for lung adenocarcinomas. *Lung* 184(6):355-362.

[19] Raidl M, Pirker C, Schulte-Hermann R, Aubele M, Kandioler-Eckersberger D, Wrba F, Micksche M, Berger W, Grasl-Kraupp B (2004). Multiple chromosomal abnormalities in human liver (pre)neoplasia. *J Hepatol* 40(4):660-668.

[20] Bown N, Cotterill S, Lastowska M, O'Neill S, Pearson AD, Plantaz D, Meddeb M, Danglot G, Brinkschmidt C, Christiansen H, Laureys G, Speleman F, Nicholson J, Bernheim A, Betts DR, Vandesompele J, Van Roy N (1999). Gain of chromosome arm 17q and adverse outcome in patients with neuroblastoma. *N Engl J Med* 340(25):1954-1961.

[21] Buganim Y, Goldstein I, Lipson D, Milyavsky M, Polak-Charcon S, Mardoukh C, Solomon H, Kalo E, Madar S, Brosh R, Perelman M, Navon R, Goldfinger N, Barshack I, Yakhini Z, Rotter V (2010). A novel translocation breakpoint within the BPTF gene is associated with a pre-malignant phenotype. *PLoS One* 5(3):e9657.

[22] Weinberg RA (1996). How cancer arises. *Sci Am* 275(3):62-70.

[23] Talmadge JE, Fidler IJ (2010). AACR centennial series: the biology of cancer metastasis: historical prospective. *Cancer Res* 70(14):5649-5669.

[24] Hanahan D, Weinberg RA (2000). The Hallmarks of Cancer. *Cell* 100: 57-70.

[25] Hanahan D, Weinberg RA (2011). Hallmarks of Cancer: The Next Generation. *Cell* 144: 646-674.

[26] Teng MWL, Swann JB, Koebel CM, Schreiber RD, Smyth MJ (2008). Immune-mediated dormancy: an equilibrium with cancer. *J Leukoc Biol* 84(4):988-993.

[27] Kim R, Emi M, Tanabe K (2007). Cancer immunoediting from immune surveillance to immune escape. *Immunology* 121(1):1-14.

[28] Murphy KM, Travers P, Walport M, Janeway C (2012). *Janeway's Immunobiology*. 8th Edition. New York: Garland Science, Taylor & Francis, Inc.

[29] den Haan JM, Arens R, van Zelm MC (2014). The activation of the adaptive immune system: cross-talk between antigen-presenting cells, T cells, and B cells. *Immunol Lett* 162(2B):103-112.

[30] van Montfoort N, van der Aa E, Woltman AM (2014). Understanding MHC class I presentation of viral antigens by human dendritic cells as a basis for rational design of therapeutic vaccines. *Front Immunol* 5(182).

[31] Chowell D, Krishna S, Becker PD, Cocita C, Shu J, Tan X, Greenberg PD, Klavinskis LS, Blattman JN, Anderson KS (2015). TCR contact residue hydrophobicity is a hallmark of immunogenic CD8+ T cell epitopes. *Proc Natl Acad Sci USA* 112(14):E1754-1762.

[32] Lieberman J (2003). The ABCs of granule-mediated cytotoxicity: new weapons in the arsenal. *Nat Rev Immunol* 3(5):361-370.

[33] Kägi D, Ledermann B, Bürki K, Zinkernagel RM, Hengartner H (1996). Molecular mechanisms of lymphocyte-mediated cytotoxicity and their role in immunological protection and pathogenesis in vivo. *Annu Rev Immunol* 14:207-32.

[34] Zaritskaya L, Shurin MR, Sayers TJ, Malyguine AM (2010). New flow cytometric assays for monitoring cell-mediated cytotoxicity. *Expert Rev Vaccines* 9(6):601-616.

[35] Qiu Z, Song C, Malakouti N, Murray D, Hariz A, Zimmerman M, Gygax S, Alhami A, Landry JW (2015). Functional interactions between NURF and Ctcf regulate gene expression. *Mol Cell Biol* 35(1):224-237.

[36] Fortier M, Caron E, Hardy MP, Voisin G, Lemieux S, Perreault C, Thibault P (2008). The MHC class I peptide repertoire is molded by the transcriptome. *J Exp Med* 205(3):595-610.

[37] Blum J, Wearsch P, Cresswell P (2013). Pathways of antigen processing. *Annu Rev Immunol* 31:443-473.

[38] Gorbulev S, Abele R, Tampé R (2001). Allosteric crosstalk between peptide-binding, transport, and ATP hydrolysis of the ABC transporter TAP. *Proc Natl Acad Sci USA* 98(7):3732-3737.

[39] Comber JD, Philip R (2014). MHC class I antigen presentation and implications for developing a new generation of therapeutic vaccines. *Ther Adv Vaccines* 2(3):77-89.

[40] Lankat-Buttgereit B, Tampé R (2002). The transporter associated with antigen processing: function and implications in human diseases. *Physiol Rev* 82(1):187-204.

[41] Rock KL, Goldberg AL (1999). Degradation of cell proteins and the generation of MHC class I-presented peptides. *Annu Rev Immunol* 17:739-779.

[42] Uebel S, Tampé R (1999). Specificity of the proteasome and the TAP transporter. *Curr Opin Immunol* 11(2):203-208.

[43] Goldberg AL, Cascio P, Saric T, Rock KL (2002). The importance of the proteasome and subsequent proteolytic steps in the generation of antigenic peptides. *Mol Immunol* 39(3-4):147-164.

[44] Tao K, Fang M, Alroy J, Sahagian GG (2008). Imagable 4T1 model for the study of late stage breast cancer. *BMC Cancer* 8:228.

[45] Pulaski BA, Ostrand-Rosenberg S (2001). Mouse 4T1 breast tumor model. *Curr Protoc Immunol* Chapter 20.2.

[46] Pulaski BA, Terman D, Khan S, Meuller E, Ostrand-Rosenberg S (2000). Cooperativity of Staphylococcal aureus enterotoxin B superantigen, major histocompatibility complex class II, and CD80 for immunotherapy of advanced metastases in a clinically relevant post-operative mouse breast cancer model. *Cancer Res* 60:2710-2715.

[47] Asiakson CJ, Miller FR (1992). Selective events in the metastatic process defined by analysis of the sequential dissemination of subpopulations of a mouse mammary tumor. *Cancer Res* 52(6):1399-1405.

[48] Oelze ML, O'Brien WD Jr, Blue JP, Zachary JF (2004). Differentiation and characterization of rat mammary fibroadenomas and 4T1 mouse carcinomas using quantitative ultrasound imaging. *IEEE Trans Med Imaging* 23(6):764-771.

[49] Youn JI, Nagaraj S, Collazo M, Gabrilovich DI (2008). Subsets of myeloid-derived suppressor cells in tumor-bearing mice. *J Immunol* 181(8):5971-5802.

[50] Overwijk WW, Restifo NP (2001). B16 as a mouse model for human melanoma. *Curr Protoc Immunol* Chapter 20.1.

[51] Bobek V, Kolostove K, Pinterova D, Kacprzak G, Adamiak J, Kolodiej J, Boubelik M, Kubecova M, Hoffman RM (2010). A clinically relevant, syngenic model of spontaneous, highly metastatic B16 mouse melanoma. *Anticancer Res* 30(12):4799-4804.

[52] Nakamura K, Yoshikawa N, Yamaguchi Y, Kagota S, Shinozuka K, Kunimoto M (2001). Characterization of mouse melanoma cell lines by their mortal malignancy using an experimental metastatic model. *Life Sci* 70(7):791-798.

[53] Strome SE, Voss E, Wilcox R, Wakefield TL, Tomada K, Flies D, Chapoval A, Lu J, Kasperbauer JL, Padley D, Vile R, Gastineau D, Wettstein P, Chen L (2002). Strategies for antigen loading of dendritic cells to enhance the antitumor immune response. *Cancer Res* 62(6):1884-1889.

[54] Miyagawa F, Gutermuth J, Zhang H, Katz SI (2010). The use of mouse models to better understand mechanisms of autoimmunity and tolerance. *J Autoimmun* 35(3):192-198.

[55] Yang M, Mine T (2009). Novel T-cell epitopes of ovalbumin in BALB/c mouse: Potential for peptide-immunotherapy. *Biochem Biophys Res Community* 378(2):203-208.

[56] Lipford GB, Hoffman M, Wanger H, Heeg K (1993). Primary in vivo responses to ovalbumin. Probing the predictive value of the Kb binding motif. *J Immunol* 150(4):1212-1222.

[57] Clarke SR, Marnden M, Kurts C, Carbone FR, Miller JF, Heath WR (2000). Characterization of the ovalbumin-specific TCR transgenic line OT-I: MHC elements for positive and negative selection. *Immunol Cell Biol* 78(2):110-117.

[58] Overwijk WW, Tsung A, Irvine KR, Parkhurst MR, Goletz TJ, Tsung K, Carroll MW, Liu C, Moss B, Rosenberg SA, Restifo NP (1998). gp100/pmel 17 is a murine tumor rejection

antigen: induction of “self”-reactive, tumoricidal T cells using high-affinity, altered peptide ligand. *J Exp Med* 188(2):277-286.

[59] Zhai Y, Yang JC, Spiess P, Nishimura MI, Overwijk WW, Robert B, Restifo NP, Rosenberg SA (1997). Cloning and characterization of the genes encoding the murine homologues of the human melanoma antigens MART1 and gp100. *J Immunother* 20(1):15-25.

[60] Hou FY, Muller AJ, Sharma MD, DuHadaway J, Banerjee T, Johnson M, Mellor AL, Prendergast GC, Munn DH (2007). Inhibition of indoleamine 2,3-dioxygenase in dendritic cells by stereoisomers of 1-methyl-tryptophan correlates with antitumor responses. *Cancer Res* 67(2):792-801.

[61] Phillipp AB, Nagel D, Stieber P, Lamerz R, Thalhammer I, Herbst A, Kolligs FT (2014). Circulating cell-free methylated DNA and lactate dehydrogenase release in colorectal cancer. *BMC Cancer* 14:245.

[62] Lin YC, Lu MC, Lin C, Chiang MK, Jan MS, Tang HL, Liu HC, Lin WL, Huang CY, Chem CM, Lai YC (2013). Activation of IFN-γ/STAT/IRF-1 in hepatic responses to Klebsiella pneumonia infection. *PLoS One* 8(11):e79961.

[63] Gao L, Wu J, Gao D (2011). Enzyme-controlled self-assembly and transformation of nanostructures in a tetramethylbenzidine/horseradish peroxidase/H2O2 system. *ACS Nano* 5(8):6736-6742.

VITA

Kristen Nichole Peterson was born on December 7, 1988 in Wexford, Pennsylvania to Richard and Kathleen Snyder. She remained in Wexford, Pennsylvania where she attended North Allegheny High School before moving to Lexington, Kentucky to study biology and psychology at the University of Kentucky. After marrying in 2011, she and her husband, Michael, moved to Richmond, Virginia where she worked at a local Environmental and Engineering Firm before receiving her acceptance into the Master's in Human and Molecular Genetics program at Virginia Commonwealth University.